Basal-Plane Functionalization of Chemically Exfoliated Molybdenum Disulfide by Diazonium Salts

Kathrin C. Knirsch,[†] Nina C. Berner,[‡,§] Hannah C. Nerl,[§,∥] Clotilde S. Cucinotta,[‡,∥] Zahra Gholamvand,[‡,∥] Niall McEvoy,[‡,§] Zhenxing Wang,[⊥,#] Irena Abramovic,[†] Philipp Vecera,[†] Marcus Halik,[⊥] Stefano Sanvito,[‡,∥] Georg S. Duesberg,[‡,§] Valeria Nicolosi,[‡,§,∥] Frank Hauke,[†] Andreas Hirsch,[†] Jonathan N. Coleman,[‡,∥] and Claudia Backes*[,‡,∥]

[†]Chair of Organic Chemistry II and Institute of Advanced Materials and Processes (ZMP), Friedrich-Alexander-Universität Erlangen-Nürnberg (FAU), Henkestraße 42, 91054 Erlangen, Germany, [‡]Centre for Research on Adaptive Nanostructures and Nanodevices (CRANN), Trinity College Dublin, Dublin 2, Ireland, [§]School of Chemistry, Trinity College Dublin, Dublin 2, Ireland, [∥]School of Physics, Trinity College Dublin, Dublin 2, Ireland, [⊥]Organic Materials & Devices (OMD), Institute of Polymer Materials, Friedrich-Alexander-Universität Erlangen-Nürnberg (FAU), Martensstraße 7, 91058 Erlangen, Germany, and [#]Advanced Microelectronic Center Aachen (AMICA), AMO GmbH, Otto-Blumenthal-Straße 25, 52074 Aachen, Germany

ABSTRACT Although transition metal dichalcogenides such as MoS_2 have been recognized as highly potent two-dimensional nanomaterials, general methods to chemically functionalize them are scarce. Herein, we demonstrate a functionalization route that results in organic groups bonded to the MoS_2 surface *via* covalent C—S bonds. This is based on lithium intercalation, chemical exfoliation and subsequent quenching of the negative charges residing on the MoS_2 by electrophiles such as diazonium salts. Typical degrees of functionalization are 10—20 atom % and are potentially tunable by the choice of intercalation conditions. Significantly, no further defects are introduced, and annealing at 350 °C restores the pristine 2H-MoS_2. We show that, unlike both chemically exfoliated and pristine MoS_2, the functionalized MoS_2 is very well dispersible in anisole, confirming a significant modification of the surface properties by functionalization. DFT calculations show that the grafting of the functional group to the sulfur atoms of (charged) MoS_2 is energetically favorable and that S—C bonds are formed.

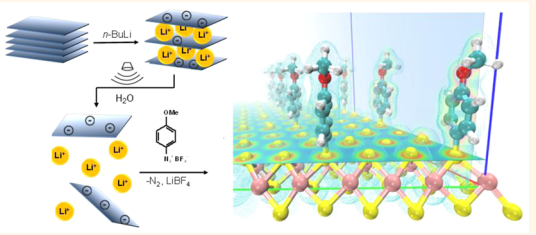

KEYWORDS: transition metal dichalcogenides · layered materials · molybdenum disulfide · covalent functionalization · basal-plane · chemical exfoliation · 1T-polytype

Over the past few years, the study of two-dimensional (2D) materials has blossomed into one of the most exciting areas of materials science.[1−7] While this field was originally driven by graphene research, more and more attention is turning to inorganic 2D materials such as MoS_2,[1] MnO_2,[7] and phosphorene.[8] This is mainly due to their diversity, their range of interesting properties and their potential in numerous applications in areas from optoelectronics to catalysis to medicine.[1−7] Currently, the 2D materials generating the most excitement are probably the family of transition metal dichalcogenides (TMDs) which include members such as MoS_2, WSe_2, and $MoTe_2$.[1,3] Significant progress has been made on the production of atomically thin, high quality TMDs by chemical vapor deposition (CVD) growth,[9,10] chemical exfoliation[3,11] and liquid phase exfoliation in suitable solvents[4,12] or by the aid of surfactants.[13,14] However, unlike the situation with graphene[15−17] or even boron nitride (BN),[18−20] there are very few reports on covalent functionalization of TMDs. Typically, functionalization of MoS_2 is achieved by ligand conjugation of thiols at sulfur vacancy sites that were either introduced by ion irradiation[21] or naturally occurring after chemical exfoliation.[22,23] Such methods are interesting but clearly limited in their utility. Up until very recently, no reaction had been reported that allows functionalization of layered MoS_2 on its basal-plane without the need of defects. There is no doubt that a general functionalization route is required as such methods have proven extremely versatile for tailoring the surface chemistry of nanomaterials. For example, chemical modification of graphene[15,16] or BN[19,20] has greatly facilitated their integration

* Address correspondence to backesc@tcd.ie.

Received for review February 11, 2015 and accepted May 13, 2015.

Published online May 13, 2015
10.1021/acsnano.5b00965

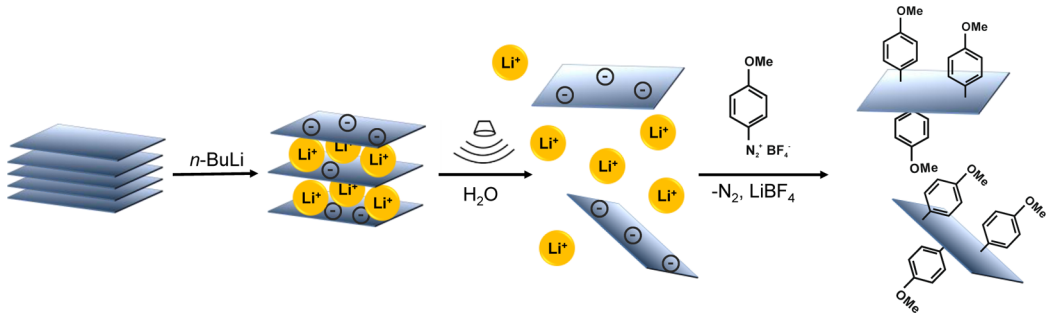

Figure 1. Schematic representation of the basal-plane functionalization of MoS_2. After intercalation with *n*-butyllithium, the negatively charged MoS_2 is dispersed in water by mild bath-type sonication leading to an efficient exfoliation into individual sheets. The charges on the MoS_2 are quenched by the addition of 4-methoxyphenyldiazonium tetrafluoroborate obtaining the functionalized product *f*-MoS_2.

into polymer matrices. In addition, functionalization can be used to sensitize initially ambipolar materials such as graphene to interact with specific molecules *via* the functional entity.[24] Furthermore, entirely new materials can be designed by attaching functional ligands such as photo- or redox-active molecules to the nanomaterial surface.[24]

With TMDs such as MoS_2, the most obvious form of covalent functionalization would be to form bonds between the functional group and the surface sulfur (or Se or Te in other TMDs). However, the basal-plane of TMDs is considered to be rather inert, making such strategies challenging. Nonetheless, as has previously been shown for BN, aggressive reagents may indeed functionalize nanomaterials that are considered inert.[19,20] As we show within this manuscript, such a strategy can also be applied to functionalize MoS_2. We expect that, once a synthetic protocol to achieve the functionalization and to characterize the material is established, the foundation will have been laid for a much broader and richer chemistry on the surface of TMDs.

The first step toward a general route to functionalize TMDs by grafting functional groups to the exposed sulfur atoms was taken by Chhowalla *et al.*, who presented a functionalization sequence based on intercalation, chemical exfoliation and subsequent quenching of the negative charges on the MoS_2 by organic halides or other strong electrophiles.[25] While the general reaction sequence is similar to the one used throughout this manuscript, there are notable and important differences in the procedure. Prior to functionalization, we tested different intercalation conditions with the goal of generating intercalated and chemically exfoliated MoS_2 with as few defects and as little structural disruption as possible. Herein, we thus show that defects are indeed not required to achieve functionalization. This also allows us to establish spectroscopic fingerprints to track the functionalization. We furthermore show that the functionalized MoS_2 is highly stable in terms of its polytype and that surface properties are significantly altered leading to a dramatically enhanced dispersibility in anisole. DFT calculations shine light on the structure and geometry of the functionalized material.

RESULTS AND DISCUSSION

Purification and Characterization of Chemically Exfoliated MoS_2. Chemical exfoliation of TMDs is generally achieved by reacting the 2D nanomaterials with *n*-butyllithium (*n*-BuLi).[3,11,26−28] This leads to the formation of a lithium intercalation compound associated with a widening of the interlayer distance between the individual MoS_2 layers and a charge transfer from *n*-BuLi to the MoS_2 (Figure 1). This, in turn, results in a (usually partial) structural reorientation of the MoS_2 from the thermodynamically more stable, trigonal prismatic, semiconducting 2H-polytype to the octahedral, metallic 1T-polytype.[3,11,26−28] In contrast to negatively charged graphene, the resultant material is reasonably stable under ambient conditions and can be dispersed in water yielding chemically exfoliated *CE*-MoS_2. Mild ultrasonication results in an almost complete exfoliation down to monolayers. In this study, we have modified the well-known intercalation procedures to give a material more suitable for subsequent functionalization (refs 3, 11, 26, 28−30 and methods). Usually in the literature, *n*-BuLi is used in excess (2.5−3 equiv *n*-BuLi per MoS_2 formula unit).[3,11,26,28,29] However, as described below, we have found the chemically exfoliated material produced using these standard conditions to be structurally defective. Since we explicitly want to develop a basal-plane functionalization of MoS_2 that does not require defects, we have modified this procedure and used excess MoS_2 in the intercalation. As we will show, the thus produced *CE*-MoS_2 is significantly less disrupted and damaged using our modified intercalation conditions.

Prior to characterization, purification of the chemically exfoliated MoS_2 is essential. In brief, organic impurities are extracted with *n*-hexane, while inorganic byproducts formed during the reaction such as LiOH are removed by several centrifugation-based washing cycles with water (for details see Methods and Supporting Information Section 2). The purified, chemically exfoliated *CE*-MoS_2, prepared using both standard

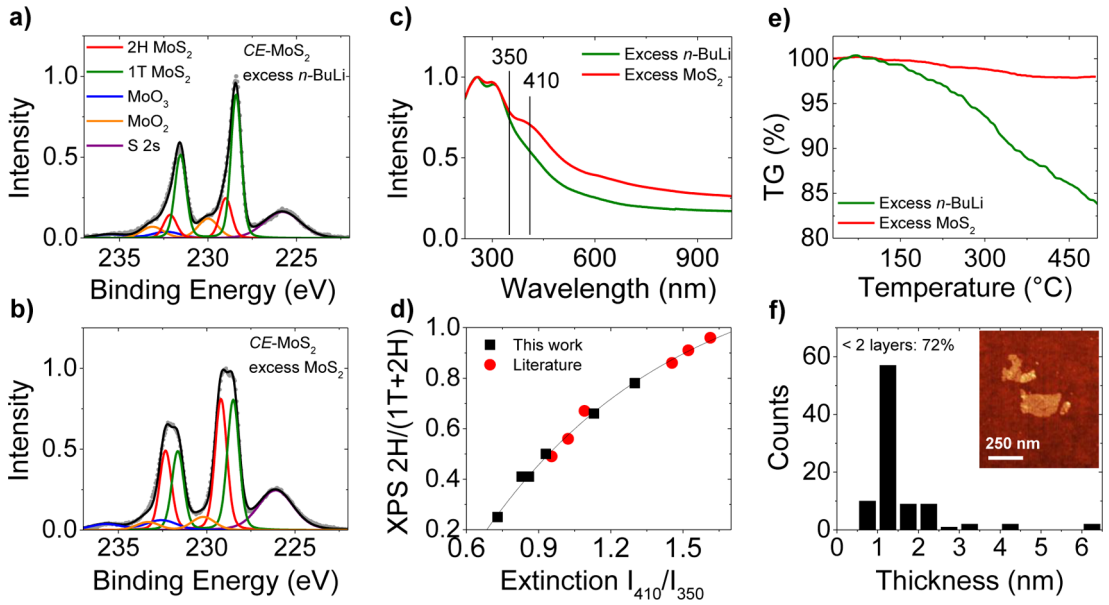

Figure 2. (a and b) Fitted Mo 3d XPS core level spectra of *CE*-MoS_2 produced using (a) excess *n*-BuLi in the intercalation and (b) excess MoS_2. Fit components are attributed to 2H-MoS_2, 1T-MoS_2, MoO_2, MoO_3, and S 2s in both cases as assigned in the figure legend in (a). The 1T content is lower in the case of the chemically exfoliated MoS_2 using excess of MoS_2 in the intercalation. (c) Extinction spectra normalized to the maximum of *CE*-MoS_2 produced using excess *n*-BuLi in the intercalation and excess MoS_2, respectively. The spectral shape is different in both cases clearly showing residual excitonic transitions of 2H-MoS_2 in *CE*-MoS_2 produced using excess MoS_2. This suggests that peak intensity ratios from extinction spectra can be used as metric for the 2H/1T content. (d) Plot of 2H/1T ratio determined from fitting the XPS Mo 3d core level spectra as a function of extinction peak intensity ratio at 410 nm/350 nm. Red data points are extracted from ref 11. The line represents an empirical asymptotic fit. (e) Thermogravimetric weight loss of *CE*-MoS_2 produced using excess *n*-BuLi in the intercalation and excess MoS_2, respectively. The significant weight loss of *CE*-MoS_2 produced using excess *n*-BuLi indicates the presence of defects. (f) Atomic force microscopy thickness histogram after drop-casting the *CE*-MoS_2 produced using excess MoS_2 onto Si/SiO_2 wafers. Seventy-two percent of the nanosheets are <2 layers with an apparent thickness <1.5 nm. Inset: representative AFM image.

intercalation procedures (*i.e.*, using excess *n*-BuLi) and our modified conditions using excess MoS_2, was subjected to X-ray photoelectron spectroscopy (XPS), extinction spectroscopy, thermogravimetric analysis (TGA), zeta potential and atomic force microscopy (AFM). While chemically exfoliated MoS_2 is commonly described as being predominantly in its 1T-polytype, we find that this depends on the experimental conditions chosen for the intercalation. Our intercalation conditions using excess MoS_2 yield *CE*-MoS_2 with a lower 1T content as revealed by the XPS Mo 3d core level spectra in Figure 2a,b. The Mo 3d core level spectra show various components that can be assigned to the 2H-MoS_2 doublet at binding energies values of 229.2 and 232.2 eV. Both spectra can be fitted with significant additional components (green curves in Figure 2a,b) shifted to lower binding energies by ~0.8 eV with respect to the main 2H-MoS_2 doublets. These components have previously been observed and identified as related to the 1T-phase of MoS_2.[11] In addition, minor contributions from oxides are detected as indicated by the blue and orange traces in the figure.[31] We further notice that a partial rearrangement to the 2H-polytype occurs more rapidly when using our modified intercalation conditions than in *CE*-MoS_2 produced from intercalation using excess *n*-BuLi (Supporting Information Section S3.1). This is unfortunate, as it renders any comparison of the chemically exfoliated precursor system and functionalized MoS_2 challenging in terms of 1T and 2H content, as this means that XPS and functionalization should be conducted the same day.

However, we have realized that XPS is not the only technique which can be used to determine the 2H/1T ratio of *CE*-MoS_2. In addition, UV−vis extinction spectra, as displayed in Figure 2c, show marked differences between the two types of *CE*-MoS_2. The extinction spectrum of 1T-MoS_2 is characterized by two transitions at 255 and 307 nm.[11] However, excitonic transitions associated with two sets of excitons are typically observed in 2H-MoS_2. These are centered between 350 and 470 nm (D and C-exciton) and 580 and 680 nm (B and A-exciton), respectively.[32] These excitonic transitions are also faintly discernible in the extinction spectra of *CE*-MoS_2 when the material has a higher 2H-polytype content, but are absent in the *CE*-MoS_2 with a high 1T content. Particularly striking is the shoulder centered at 410 nm as indicated in Figure 2c.

Such spectral changes can be expressed as peak intensity ratios, as we have previously shown for 2H-MoS_2.[14] We therefore suggest that such a peak intensity ratio can also be used to quantify the 2H/1T ratio in *CE*-MoS_2. To test this, we determined the 2H/1T ratio according to XPS on a number of samples and

measured extinction spectra the same day the XPS was acquired. We plot the 2H/1T content as a function of peak intensity ratio in Figure 2d. We chose the peak intensity ratio at 410 nm (strong contribution from 2H MoS_2) to 350 nm (strong contribution from 1T MoS_2, local minimum in 2H) as potential metric ratio. We find a very well-defined relationship relating the 2H/1T ratio (expressed as 2H/(2H + 1T)) to the intensity ratio I_{410}/I_{350} according to eq 1:

$$\frac{2H}{2H+1T} = 1.29 - 2.562 \times 0.287^{x} \qquad (1)$$

where x is the extinction intensity ratio.

Importantly, data extracted from the literature[11] falls on the same curve, strongly suggesting that this peak intensity ratio based in the extinction spectra can indeed be used as a metric to quantitatively determine the 2H/1T polytype content of *CE*-MoS_2. This will be important for the analysis of the functionalized material further down below (also see Supporting Information section 3.5).

As already mentioned above, we nonetheless consider the chemically exfoliated MoS_2 produced from our modified intercalation conditions using excess MoS_2 to be a better precursor for the subsequent functionalization than the material produced from using excess *n*-BuLi, as the latter is structurally less intact. This is best visualized from the thermogravimetric analysis presented in Figure 2e. The *CE*-MoS_2 using our modified reaction conditions (2H/(2H + 1T) = 0.5−0.6) only shows a minor weight loss of 2% in the temperature range of 25−500 °C compared to >15% in the case of intercalation using excess of *n*-BuLi (2H/(2H + 1T) = 0.25). This suggests a significant disruption of the MoS_2 structure when using excess *n*-BuLi (also see Supporting Information Figure S3.2) in the intercalation. Transmission electron microscopy (TEM) analysis confirms that considerable damage is done to the MoS_2 nanosheets when using these standard conditions (Supporting Information Figure S3.3). Since our aim is to functionalize MoS_2 which is as structurally perfect as possible, we intercalate using excess MoS_2 throughout the remainder of this study.

We anticipate that an efficient functionalization using electrophiles will depend on two factors: the negative surface charge residing on the MoS_2 and the available surface area which depends on the degree of exfoliation. The measured zeta potential of −48 mV (Supporting Information Figure S2.2) shows that the MoS_2 nanosheets are indeed negatively charged. The degree of exfoliation was estimated using atomic force microscopy (Figure 2f for representative image) after drop-casting the dispersion on Si/SiO_2 wafers. This showed that 72% of the chemically exfoliated nanosheets displayed an AFM height of <1.5 nm consistent with mono- and bilayered species (see histogram in Figure 2f).[11,33,34] The mean length of the nanosheets was determined to be 180 nm with a length/width ratio of ∼2. The degree of exfoliation in our chemically exfoliated MoS_2 is slightly lower than that in some cases reported in literature.[11,35] However, a direct comparison with literature is not possible, as the degree of exfoliation of *CE*-MoS_2 in water depends on a number of factors such as MoS_2 starting material, details of sonication and purification and potentially the intercalation conditions. Importantly, the degree of exfoliation using our modified intercalation conditions is similar to that obtained from intercalation using the standard conditions when applying identical purification and sonication protocols (Supporting Information Section 3.4). We thus conclude that our exfoliated *CE*-MoS_2 produced from the modified, much milder intercalation conditions is an ideal precursor for covalent functionalization.

Functionalization of *CE*-MoS_2. Since MoS_2 has long been considered to be unreactive and almost inert even after intercalation, we have chosen very aggressive electrophiles, namely diazonium salts (in this case 4-methoxyphenyldiazonium tetrafluoroborate) to quench the negative charges on the MoS_2 and functionalize the material. Diazonium salts have extensively been used in carbon allotrope functionalization and represent a versatile and rich class of suitable electrophiles for reaction with MoS_2.[17,36−38] After addition of the diazonium salt, we observe an immediate precipitation of black powder from the yellowish-brown dispersion in water, pointing to an efficient quenching of the charges. As we will show below, this is accompanied by a basal-plane functionalization of MoS_2 to generate *f*-MoS_2. Our XPS and IR spectroscopic analysis strongly suggests that partial negative charges on the S in the *CE*-MoS_2 are neutralized by the addition of the cationic electrophile resulting in the formation of a S−C bond. Owing to the high degree of exfoliation of the *CE*-MoS_2 precursor, both sides of the nanosheets are accessible for potential functionalization in dispersion. However, as we also show, this is not a prerequisite for the functionalization, as it can also be achieved after deposition on a substrate (Supporting Information Section 7.3).

Bulk Characterization of Functionalized MoS_2. The immediate flocculation of MoS_2 after addition of diazonium salt due to the quenching of the charges residing on the nanosheets is confirmed by zeta potential measurements (Supporting Information Figure S4.1). These show that by 2 min after addition of the diazonium salt, the zeta potential increases from −48 mV to 0. The resultant powder was filtered, washed with water and isopropyl alcohol, and dried before being subjected to thermogravimetric analysis coupled to mass spectrometry (TGA-MS), Raman and IR spectroscopy and XPS as described below.

Thermogravimetry showed no mass loss below 220 °C followed by a 7% mass reduction in the temperature range 220−450 °C (Figure 3a). As small, van der Waals bonded molecules tend to desorb from

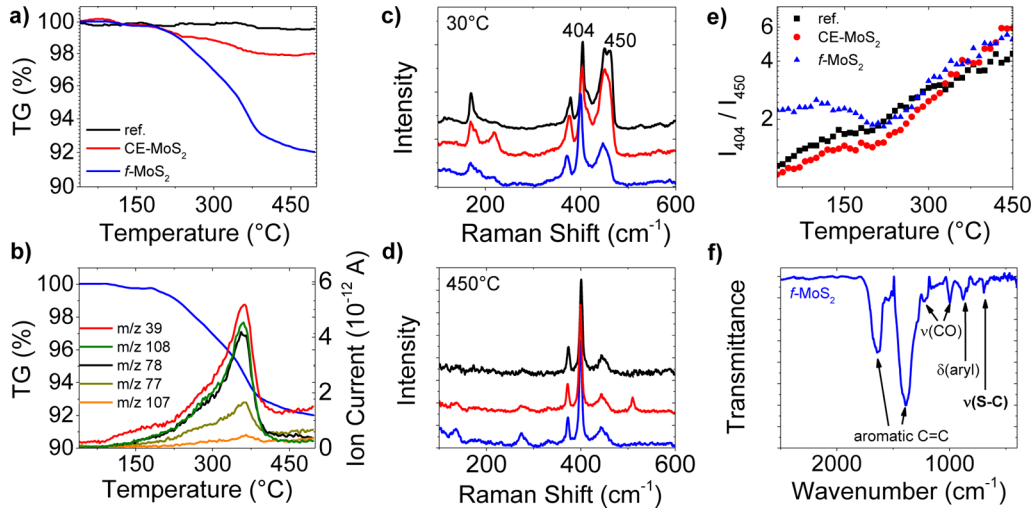

Figure 3. (a) Thermogravimetric weight loss of the untreated MoS_2, the *CE*-MoS_2 and the material after functionalization. The weight loss of 6.7% in the temperature regime of 220−450 °C corresponds to a bulk degree of functionalization of 10% per MoS_2 unit. (b) Detected mass fragments of *f*-MoS_2 corresponding to methoxybenzene (*m/z* 107, 108), benzene (*m/z* 39, 77, 78), demonstrating that the mass loss in the temperature range of 200−450 °C is due to grafting of the functional group. (c and d) Raman spectra (633 nm excitation, average of 250 individual spectra) of the MoS_2 reference, *CE*-MoS_2 and *f*-MoS_2 normalized to the A_{1g} mode at 404 cm^{-1} (offset for clarity). Figure legend as in (a). (c) Spectra measured at 30 °C. The second-order longitudinal acoustic phonon (2LA(M) at 450 cm^{-1}) appears decreased in the *f*-MoS_2. (d) Spectra measured at 450 °C. (e) Plot of the Raman intensity ratio of the A_{1g} mode to the 2LA(M) mode of the MoS_2 reference, *CE*-MoS_2 and *f*-MoS_2 as a function of temperature. The reference and the *CE*-MoS_2 follow a very similar trace, while the *f*-MoS_2 deviates significantly at temperatures below 220 °C exhibiting a higher A_{1g}/2LA(M) ratio. This suggests that this peak intensity ratio can be used as indicator for successful functionalization. (f) FTIR spectrum (measured in diffuse reflectance mode with CsI as matrix) of *f*-MoS_2. The vibrational modes of the functional group can be clearly identified. In addition, a vibration at 695 cm^{-1} is detected that can be assigned to a S−C stretching vibration.

surfaces below 200 °C,[39] this suggests the mass loss to be associated with species which are strongly bonded to the surface or intercalated between restacked sheets.[40] To test whether the mass loss is due to diazonium salt trapped between restacked layers or noncovalently adsorbed on the MoS_2, we performed reference experiments using liquid exfoliated[12] uncharged MoS_2 (Supporting Information, Section 6). No significant weight loss was observed in the reference experiments, confirming that physisorption and trapping between restacked MoS_2 nanosheets is negligible. Significantly, thermogravimetric analysis coupled to mass spectrometry (TGA-MS) allows the association of the moieties which had thermally detached from the functional group or its fragments, respectively (Figure 3b). Five main mass fragments with *m/z* = 107, 108 (methoxybenzene), *m/z* = 77, 78 (benzene), and *m/z* = 39 (doubly charged benzene ring) were detected peaking at 360 °C, clearly evidencing that the mass loss is due to the detachment of the functional group. Assuming that the weight loss in this temperature regime stems from the functional group itself, we use the associated mass loss of 7% to determine that every 10th MoS_2 unit bears ∼1 functional moiety, *i.e.*, the bulk degree of functionalization is 10% per MoS_2 unit.

Since Raman spectroscopy is a commonly used and powerful tool in nanomaterial characterization, we reasoned that Raman spectra may contain information on the functionalization. The Raman spectrum of MoS_2 when excited off resonance (*e.g.*, λ = 532 nm) is quite well understood and characterized by two main phonon peaks (the A_{1g} at 404 cm^{-1} and E^1_{2g} mode at 380 cm^{-1}). However, when resonantly excited with a red laser (633 nm), a number of second order modes is observed and the spectrum is rich in additional features that are not fully understood[10,41−45] (for a detailed discussion see Supporting Information Section 4.2.1). We can nonetheless use the Raman spectrum to trace differences between the MoS_2 reference powder, the chemically exfoliated precursor and the *f*-MoS_2. Low temperature spectra (30 °C) are displayed in Figure 3c. The spectra are the mean of 250 individual spectra acquired on the respective powder to account for local sample inhomogeneity and changes of the laser focus. Two notable differences between the samples are observed: first, the J1-J3 phonon modes (170−300 cm^{-1}) attributed to the 1T phase of MoS_2[46] are clearly discernible in the chemically exfoliated material, while basically absent in the *f*-MoS_2 and the powder reference. However, at elevated temperatures, they also appear in the *f*-MoS_2 (Supporting Information Figures S4.3 and S4.4) suggesting that they are suppressed in the room temperature spectrum of *f*-MoS_2 even though the MoS_2 is still in its 1T conformation. The second pronounced change in the low temperature Raman spectra is the intensity ratio of the A_{1g} mode at 404 cm^{-1} to the 2LA(M) mode at 450 cm^{-1}. (NB: The peak at 450 cm^{-1} contains multiple components. But for the sake of simplicity we refer to it as the 2LA(M) mode.) This intensity ratio is significantly higher in the

functionalized sample compared to the chemically exfoliated precursor and the starting powder, suggesting that the 2LA(M) mode is also suppressed in *f*-MoS_2. To confirm that this change in intensity ratio is attributed to the functionalization, we performed temperature dependent Raman spectroscopy monitoring the evolution of the Raman spectra (mean of 250 spectra each) when heating the sample from room temperature to 500 °C in 10 °C intervals. At high temperatures (450 °C, Figure 3d), all features attributed to the 1T-polytype have disappeared and the spectra of reference, chemically exfoliated and functionalized MoS_2 are identical suggesting that no permanent harm to the lattice was done by intercalation and functionalization.

To test whether the intensity ratio A_{1g}/2LA(M) is indicative for functionalization, we plot this ratio as a function of temperature in Figure 3e. Both the *CE*-MoS_2 and the reference powder follow a similar trace (even though there are differences when looking at individual components as discussed in the Supporting Information Section 4.2.3). Significantly, the *f*-MoS_2 exhibits a higher A_{1g}/2LA(M) intensity ratio for temperatures up to 220 °C. This coincides with the temperature where the cleavage of the functional group starts according to TGA-MS. We thus propose that this intensity ratio can indeed be used as an indicator for the functionalization of MoS_2. However, we note that a detailed understanding is beyond the scope of this manuscript.

The presence of the functional group is further evidenced by IR spectroscopy (Figure 3f). The pattern of the aryl bending mode at ~880 cm^{-1} suggests a 1,4-substitution pattern on the benzene ring consistent with anchoring of the functional group in *para* position to the methoxy-group.[47] Most importantly, a vibration at ~695 cm^{-1} is observed which can be assigned to a S−C stretching vibration strongly suggesting the functional group to be anchored to S atoms of the MoS_2. In addition, we note that no characteristic N_2^+ vibration (expected at 2300 cm^{-1}) of the diazonium salt precursor is detected. This indicates that physisorption or intercalation of the precursor salt only occurs to a very minor extent and is not detectable. Annealing at 500 °C to remove the functional groups showed the IR spectra of both *f*-MoS_2 and *CE*-MoS_2 to return to that of the MoS_2 starting powder (Supporting Information Figure S4.6). This evidences that the functionalization is fully reversible and the intact MoS_2 can be restored further supporting the conclusion from the Raman spectra.

X-ray Photoelectron Spectroscopy (XPS). The data presented above clearly provides evidence for successful grafting of the functional group to the MoS_2 scaffold. IR spectroscopy suggests the formation of a C−S bond. However, IR alone cannot provide unambiguous proof of a covalent functionalization. We have therefore turned to X-ray photoelectron spectroscopy to distinctively probe the chemical environment of the Mo and S, respectively. The fitted Mo 3d and S 2p core level spectra of the MoS_2 reference powder, the *CE*-MoS_2 precursor, the *f*-MoS_2 and the defunctionalized material (after annealing, *df*-MoS_2) are presented in Figure 4. We note that we did not observe any other elements in the survey spectra than Mo, S, C, and O (Supporting Information Table S1).

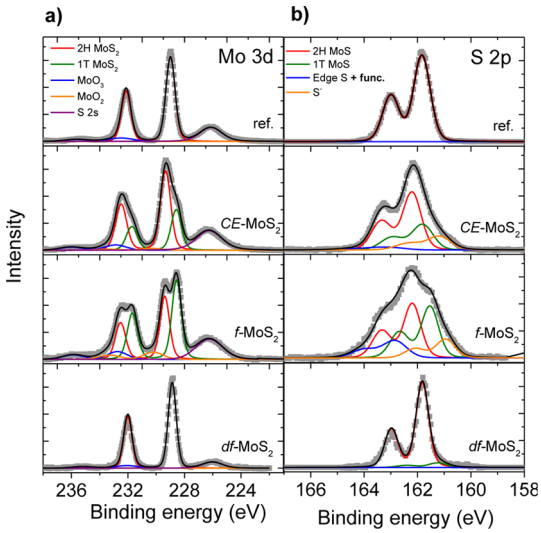

Figure 4. From top to bottom: Fitted XPS core level spectra of the MoS_2 powder, chemically exfoliated *CE*-MoS_2 (produced from using excess MoS_2 in the intercalation), functionalized *f*-MoS_2, and defunctionalized *df*-MoS_2 (after annealing). (a) Mo 3d core level, (b) S 2p core level. The reference is perfectly consistent with 2H-MoS_2, while intercalation yields a mixture of 2H- and 1T-MoS_2 (with a very minor contribution stemming from oxides as indicated by the orange and blue fit lines in the Mo 3d core level). Functionalization gives rise to a component at higher binding energies in the S 2p core level spectra. The 2H/1T ratio of *CE*-MoS_2 and functionalized *f*-MoS_2 is different due to rapid rearrangement of 1T-MoS_2 from our intercalation using excess MoS_2 (see SI). The degree of functionalization estimated from the integrated areas of the individual components in the S 2p core level spectra is consistent with the 10% calculated from TGA. After annealing, the MoS_2 is restored to its pristine 2H polytype.

Both S 2p and Mo 3d core level spectra (Figure 4) show the *CE*-MoS_2 and *f*-MoS_2 to be a mixture of 1T- and 2H-MoS_2. Accordingly, the 1T phase was preserved during the functionalization. We note that the 2H/1T ratio of the *CE*-MoS_2 precursor and the *f*-MoS_2 is slightly different. While the 2H/1T ratio of *f*-MoS_2 according to the Mo 3d core level spectra is 0.45, we determined a value of 0.66 in case of the *CE*-MoS_2 (see Supporting Information Table S1). We note that our extinction spectra 2H/1T metric suggests that the 2H/1T ratio of the chemically exfoliated precursor at the time the functionalization was performed was 0.45 (Supporting Information Section 3.5). However, XPS on the *CE*-MoS_2 was acquired 1 week later and structural rearrangement to the 2H-polytype had already occurred. While this relatively quick partial rearrangement from 1T- to 2H-polytype using our milder, modified intercalation conditions is unfortunate, we nonetheless found the

benefits from this modified intercalation (such as lower defect content) to be beneficial over the standard literature conditions when it comes to studying functionalization. Furthermore, the results suggest that the 1T-polytype is stabilized by the functionalization, as no rearrangement to the 2H-polytype was observed in the time frame of one month (Supporting Information Section 4.4 and Table S1).

After annealing, the pristine 2H-MoS_2 is completely recovered, consistent with the observation from IR and Raman spectroscopy. While no differences in the Mo 3d core level spectra are observed (other than varying 2H/1T contents), the S 2p core level spectra are distinct in *CE*-MoS_2 and *f*-MoS_2 (Figure 4b). The S 2p core level spectra of the *CE*-MoS_2 can be fitted with four components: 2H-MoS_2, 1T-MoS_2, a species previously observed in surfactant-exfoliated 2H-MoS_2 associated with edges of the flakes (shifted by ~0.7 eV to higher binding energies relative to 2H-MoS_2)[14] and a component at lower binding energies (~1.2 eV relative to 2H-MoS_2) most likely stemming from electron-rich sulfur from the electron transfer of *n*-BuLi during the intercalation. In the functionalized *f*-MoS_2, the electron-rich sulfur species at lower binding energies decreases in favor of a significantly increased percentage of the "edge-S" component at higher binding energies. This is more pronounced for material obtained from intercalation using excess *n*-BuLi, Supporting Information Section 7.1. This strongly suggests that any (partial) charges on the sulfur atoms of the chemically exfoliated *CE*-MoS_2 are neutralized by grafting of the functional groups to the sulfur atoms as observed in zeta potential measurements. We can use the integrated areas of the fit components to estimate the degree of functionalization on the basis of XPS. In the *CE*-MoS_2, 4% of the total sulfur component is attributed to the edge component sulfur at higher binding energies. In turn, in the functionalized *f*-MoS_2, the latter is increased to 15%. The degree of functionalization can thus be determined to be 11% per sulfur atom. This coincides with the degree of functionalization obtained from TGA-MS (10% per MoS_2 unit). Nominally, this appears contradictory, as XPS probes the degree of functionalization on the S atoms, while TGA yields values related to the MoS_2 unit. However, since S atoms bridge the Mo atoms, if every 10th MoS_2 unit bears a functional group, this also means that roughly every 10th sulfur is functionalized. We would like to emphasize that the experimentally observed degree of functionalization of 10% can only be achieved if the functionalization occurs at the basal-plane rather than edge sites only. However, it is currently unclear whether edge sites are also affected, or even preferentially functionalized due to their anticipated higher reactivity.

We note that a basal-plane functionalization of MoS_2 involving the formation of S−C bonds after intercalation-based activation of the MoS_2 differs significantly from recent functionalization routes,[22,23] where S vacancies were filled by coordinating thiols to chemically exfoliated MoS_2. We are convinced that our route has significant advantages, as it is not limited by the presence of such vacancies and can be applied even to MoS_2 of the highest quality. In addition, the functionalization by forming a covalent bond is in marked contrast to the formation of intercalation compounds from chemically exfoliated MoS_2. This is further illustrated by wide-angle X-ray diffraction confirming the absence of 00*l* reflections in the *f*-MoS_2 (Supporting Information Figure S4.8) and the absence of long-range order along the *c*-axis in contrast to intercalation compounds (see ref 26 and references therein).

Dispersibility and Structural Integrity of the Lattice. An important point of the functionalization of nanomaterials in general is the alteration of the surface properties due to the attachment of functional moieties. This is expected to change the surface energy of the nanomaterial and as a consequence its dispersibility.[48] To test this, we have dispersed the MoS_2 reference powder, the *CE*-MoS_2, *f*-MoS_2 (both after filtration and drying) and the defunctionalized *df*-MoS_2 in *N*-methyl-2-pyrrolidone (NMP) and anisole. NMP is known to be a good solvent for MoS_2 with surface energies and solubility parameters matching those of the nanomaterial.[12,48,49] In turn, anisole (methoxybenzene) is chemically well-matched to our functional group. Photographs of the dispersions obtained after mild bath sonication (20 min) and centrifugation at 500 rpm (28 *g*) are depicted in Figure 5a,b. We note that the MoS_2 powder is not a suitable reference for the dispersibility study, as it has a significantly different morphology. Since the crystallites were not broken up by any pretreatment (*i.e.*, chemical exfoliation), much more energy would be required to efficiently disperse the powder even in good solvents such as NMP. However, for this study, we wanted to keep the sonic energy input to a minimum to avoid potential defunctionalization due to strong local heating during sonication. As expected, the dispersibility of *f*-MoS_2 is significantly altered: compared to the defunctionalized material, the concentration of dispersed *f*-MoS_2 is lower by approximately a factor of 3 in NMP. In turn, *f*-MoS_2 is well dispersible in anisole unlike the chemically exfoliated and defunctionalized MoS_2. This suggests that a degree of functionalization of 10% is already sufficient to significantly alter the surface energy of the MoS_2. In addition, this indirectly evidences that the basal-plane is reasonably homogeneously decorated with a neutral functional moiety. If a charge transfer complex between diazonium reagent and *CE*-MoS_2 was formed, no such enhanced dispersibility in anisole would be expected.

The extinction spectra of the NMP dispersions are displayed in Figure 5c. The spectrum of the MoS_2 powder is consistent with bulk 2H-MoS_2 showing the characteristic excitonic transitions.[12,14,32] The spectrum of the defunctionalized material resembles that of very

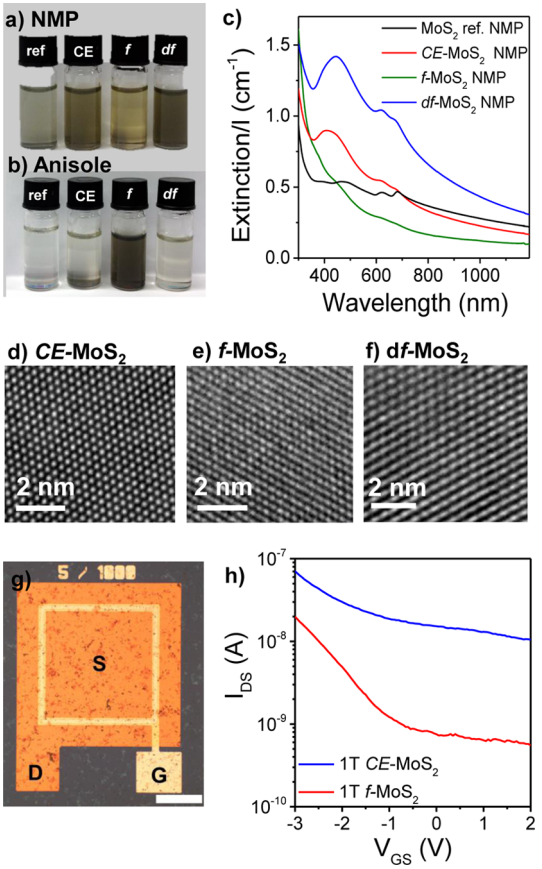

Figure 5. (a and b) Redispersion of MoS_2 powder, *CE*-MoS_2, functionalized *f*-MoS_2, and defunctionalized *df*-MoS_2 in (a) *N*-methyl-2-pyrrolidone (NMP) and (b) anisole. Chemically exfoliated and defunctionalized MoS_2 are well dispersible in NMP, while the *f*-MoS_2 is dispersible in anisole opposed to the chemically exfoliated and defunctionalized counterparts demonstrating a change in solubility parameters due to the functionalization. (c) Extinction spectra of the dispersions shown in (a) (after mild centrifugation at 500 rpm). Notably, all excitonic transitions are suppressed in *f*-MoS_2. (d–f) High resolution transmission electron microscopy (TEM) of the drop-casted dispersions in (a) showing the intact lattice of (d) *CE*-MoS_2, (e) *f*-MoS_2, and (f) *df*-MoS_2. (g and h) Electrical characterization of network devices. (g) Device image with source, drain, and gate electrodes indicated with S, D, and G. The scale bar is 100 μm. The channel length and width of the device are 5 and 1000 μm. (h) The device transfer curves before and after functionalization. Current on/off ratio increases from 6.7 (before) to 36.1 (after), indicating an enhancement in the semiconducting property.

small 2H-MoS_2 nanosheets[14,50] in analogy to spectra obtained from annealed MoS_2.[11] The spectrum of the redispersed *CE*-MoS_2 resembles a mixture of 2H- and 1T-MoS_2.[11] Since the C- and D excitonic transitions centered at 450 nm are slightly better resolved than in the initial chemically exfoliated material in water (Figure 2c), we suspect that local heating in the sonication-based redispersion resulted in a partial reconstruction of the 1T- to the 2H-phase. Most interestingly, all excitonic transitions are suppressed in the functionalized material so that optical extinction spectroscopy provides a very quick tool to determine whether functionalization was successful. This also further confirms that the electronic structure of *f*-MoS_2 is significantly different from chemically exfoliated or nonfunctionalized MoS_2. A more detailed discussion of the redispersion study is presented in the Supporting Information (section 5).

To confirm that our subsequent intercalation and functionalization sequence does not structurally harm the MoS_2 lattice, we performed a series of high resolution transmission electron microscopic investigations on the MoS_2 reference powder, *CE*-MoS_2, *f*-MoS_2 and the defunctionalized material (Figure 5d–f and Supporting Information Figure S5.5). For this purpose, grids were cast from the NMP dispersions after mild sonication and centrifugation. We note that, in all cases, the MoS_2 is only reasonably well exfoliated and appears as reaggregated agglomerates of formerly individualized nanosheets (see AFM Figure 2f and TEM Supporting Information Figure S3.3). This is attributed to the very gentle redispersion and centrifugation conditions that were chosen to avoid any structural changes of the chemically exfoliated and functionalized MoS_2. Because of that, many small patches were frequently observed on the basal-plane of the redispersed material (center images in Supporting Information Section S5.5). However, apart from that, the lattice is intact over wide regions (Figure 5d–f) showing that no severe structural damage to the MoS_2 was induced by our functionalization sequence. We note that an analysis of 2H- and 1T-polytype content from bright field images is extremely challenging[51] and beyond the scope of the manuscript.

Functionalization after Intercalation with Excess *n*-BuLi. The intercalation conditions with excess MoS_2 have proven to be ideal for establishing the characterization protocols to trace the subsequent basal-plane functionalization. However, this *CE*-MoS_2 has the disadvantage of undergoing a rather rapid rearrangement from its 1T-polytype to its 2H-polytype. It is therefore very challenging to compare, for example, electrical properties of *f*-MoS_2 to the *CE*-MoS_2 precursor, as the 2H/1T ratio may vary. Given that the functionalization stabilizes the 1T-phase, which is known to be metallic in chemically exfoliated MoS_2, it is important to test whether this is also the case for *f*-MoS_2. We have therefore performed functionalization of 1T *CE*-MoS_2 from intercalation using excess *n*-BuLi. A detailed characterization is presented in the Supporting Information (Section 7). The XPS analysis shows that only very minor 2H/1T rearrangement occurs within one month (Supporting Information Section 7.1). The initial 1T/2H ratio was determined to be ~4 (*via* Mo 3d core level X-ray photoelectron spectra, Supporting Information Table S2). Thus, both chemically exfoliated and functionalized MoS_2 can be considered to be predominantly 1T-MoS_2. XPS furthermore suggests that the degree of functionalization is 20%.

To test the electrical characteristics of 1T *CE*-MoS_2 and 1T *f*-MoS_2, we have fabricated field-effect transistors

(FETs) based on self-assembled monolayers (SAMs) using region-selective deposition of the chemically exfoliated MoS_2. This technique has previously been applied for electrical characterization of functionalized carbon allotropes and is described in detail elsewhere.[52,53] In brief, the network devices were produced by immersing prepatterned chips covered with a positively charged SAM in the channel region (3-methyl-1-(12-phosphonododecyl)imidazolium bromide) in an aqueous dispersion of the 1T *CE*-MoS_2. Due to Coulombic attraction, 1T *CE*-MoS_2 nanosheets are selectively deposited in the channel region (Figure 5g).[54] The network transistor of the chemically exfoliated MoS_2 is difficult to turn off and shows on/off ratios of ~7 due to the metallic nature of 1T-MoS_2. After testing, the device was soaked in an aqueous solution of the diazonium salt for 5 min. Successful functionalization was confirmed by Raman spectroscopy (Supporting Information Figures S7.4 and S7.5). The transistor showed a clear improvement in on/off ratios (up to ~36) suggesting that the *f*-MoS_2 exhibits semiconducting properties even though the 1T-polytype is maintained (Figure 5h). The device exhibits a typical p-type characteristic which could be due to the electrostatic doping from the SAM layer underneath.[54] The hole mobility decreased from 3.9×10^{-4} $cm^2/(V\ s)$ before functionalization to 1.2×10^{-4} $cm^2/(V\ s)$ after functionalization. This could be attributed to the extra scattering centers introduced by the functionalization. However, we have to note that the decrease is not pronounced at all and the electric property of the network transistor is largely preserved.

Modeling. To gain further insights in the structure and bonding in the functionalized MoS_2, we have performed density functional theory (DFT) calculations. We propose a reaction model implying dissociative chemisorption of *n* (number of molecules) 4-methoxyphenyldiazonium cations on a MoS_2 surface with net charge of $-|e|n$, producing the release of *n* N_2 molecules. To test whether steric hindrance may occur for degrees of functionalization of 20% per MoS_2 unit, functionalized surfaces with low and high coverage have been modeled being equivalent to grafting one or four molecules ($n = 1$ or 4) per MoS_2 unit cell, respectively.

The reaction energy is evaluated as

$$E_{react} = [E_{MoS_2} + nE_{cat}] - [E_{funct} + nE_{N_2}]$$

where, *n* is the number of chemisorbed molecules, E_{MoS2} and E_{funct} are the energies of the clean and the functionalized surfaces, respectively and E_{cat} and E_{N2} are the energies of the isolated cation and the released N_2 molecule. The reaction is largely energetically favorable, with a reaction energy of E_{react} = 2.33 eV per molecule at low coverage. At high coverage, the reaction energy per molecule becomes even larger. We note that this reaction energy is much larger than calculated adsorption energies for physisorbed molecules which are in the range of 0.5 eV per molecule.[55]

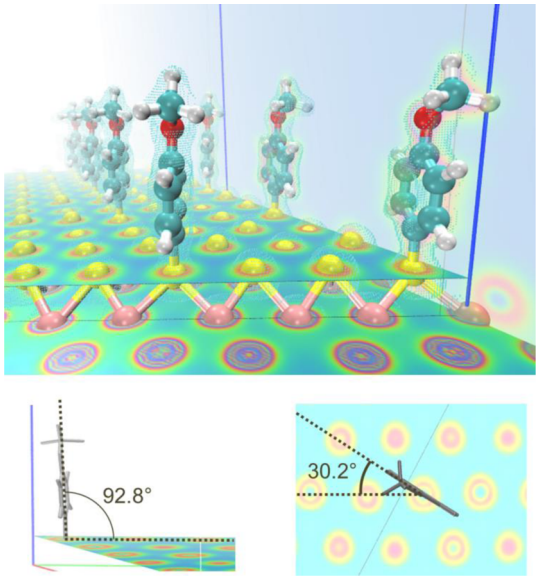

Figure 6. (Top) Ball and stick representation of the functionalized monolayer with high coverage. Red, blue, yellow, pink, and white balls represent O, C, S, Mo, and H atoms, respectively. The dotted area reproduces the total electronic charge (isosurface with a contour level of 0.8 electrons). The two (001) planes (perpendicular to *z*-axis) depict volume slices of the total electronic charge on Mo (below) and S (above) surfaces. (010) plane is also highlighted by a transparent slice. The position of this plane along the *y*-axis is highlighted by the thin gray line perpendicular to (001) plane, corresponding to where S−C bonds lie. Red and blue on the planes indicate high and low charge values, respectively. (Bottom left) Tilt angle between *y* and molecular axis. (Bottom right) Dihedral angle between molecular plane and (100) surface. In both panels, the molecule is schematically sketched and the electron charge on the reference grafting S plane at low coverage is also represented. The *y*-axis is represented in top and bottom right insets by a gray line lying on the (001) plane. In bottom left inset, red, green, and blue lines represent *x*-, *y*-, and *z*-axis, respectively.

This suggests that, even though physisorption may occur, the reaction is thermodynamically driven toward a covalent functionalization. This agrees well with our experimental data from TGA-MS showing that the mass fragments attributed to the functional group are detected in a temperature range of 270−450 °C with only traces being detected at lower temperatures where physisorbed species would be expected.

After geometry relaxation, the 1T-MoS_2 monolayer shows a 2×1 reconstruction, known as *1T′* phase (see Supporting Information Section 8). In the charged MoS_2 parent system, we observe a bidental Mo−S bonds distribution (centered around 2.42 and 2.48 Å, respectively). This structure relaxes after functionalization in such a way that all Mo−S bonds are distributed around an average Mo−S bond length of 2.45 Å. The grafted molecule is approximately perpendicular to the surface (92.8°) (Figure 6, bottom left) and the dihedral angle between molecular plane and (100) surface is 30.22° (Figure 6, bottom right). The analysis of the electronic structure of the clean and functionalized

monolayer shows that they are both semiconductors with a very tiny band gap (see Supporting Information Section 8).

The analysis of the Bader charges[56] of the clean (uncharged and nonfunctionalized) MoS_2 system shows a charge polarization with S atoms bearing partial negative charges and Mo atoms being partially positively charged (quantitative analysis see Supporting Information Section 8). When excess charges are added to the overall neutral system (such as experimentally achieved after intercalation with *n*-BuLi), these distribute over the external S atoms. This is rather important, as a chemical reaction with a positively charged reagent is likely to occur on the negatively charged reaction site, *i.e.*, the S atoms. The Coulombic attraction between the negatively charged S surfaces and the positively charged diazonium reagent also accounts for the spontaneous reaction experimentally observed and the strongly negative reaction energy. Our calculations confirm that S−C chemical bonds are formed. The C atom grafted to the surface withdraws 0.15 $|e|$ from its neighbor S, which is about 0.2 $|e|$ less charged than the other surface S atoms. A very similar picture is observed when the coverage is higher (Figure 6, top).

This clearly confirms the experimental observations that basal-plane functionalization on the S atoms of chemically exfoliated MoS_2 is readily accessible by reaction of *CE*-MoS_2 with strong electrophiles such as diazonium salts.

CONCLUSION

In conclusion, we have demonstrated a novel functionalization sequence for transition metal dichalcogenides such as MoS_2. The functionalization is based on reacting intercalated, chemically exfoliated MoS_2 with electrophiles such as diazonium salts. The use of chemically exfoliated MoS_2 is beneficial due to the good exfoliation in water making both sides of the nanosheets accessible. This yields typical degrees of functionalization of 10−20 atom %. The successful functionalization was evidenced by zeta potential measurements, IR, Raman and extinction spectroscopy, TGA-MS and XPS.

The basal-plane functionalization is fully reversible and annealing restores predominantly pristine 2H-MoS_2. High resolution TEM confirms the lattice to be widely intact. The basal-plane functionalization furthermore yields *f*-MoS_2 with different surface properties or surface energies which is reflected in an enhanced dispersibility in solvents that are compatible with the functional group. In the functionalized MoS_2, the 1T-polytype that is typical for intercalated MoS_2 is maintained and even stabilized. However, in contrast to intercalated 1T-MoS_2 which is known to be metallic, *f*-MoS_2 exhibits semiconducting properties as concluded from electrical characterization of network transistor devices before and after functionalization. DFT calculations show that the reaction is energetically very favorable and that a S−C bond is formed.

We believe this work is important, as it establishes spectroscopic fingerprints of covalently functionalized MoS_2. We also show that this method is intrinsically not reliant on the presence of defects or vacancies and so can potentially be applied to high-quality nanosheets. In addition, the method is versatile, with functionalization achievable both in solution and for nanosheets deposited on surfaces. Importantly, this approach is not limited to MoS_2 but is applicable to any TMD (or indeed any layered compound) which can be intercalated with lithium. We anticipate that this ability to easily functionalize TMDs is only the first step toward the development of secondary functionalization routes leading to the bonding of complex molecular systems to the nanosheet surface.

METHODS

Sample Preparation. More details on materials and methods are presented in the Supporting Information.

Synthesis of Diazonium Compound. In a 500 mL three neck flask equipped with a stir bar, gas outlet ,and a dropping funnel 10 g (81 mmol) *p*-anisidine were suspended in 250 mL water. Six g (89 mmol) sodium nitrite was added, and the suspension was cooled with an ice bath. Dropwise addition of 50 mL (36 g, 48 wt % in H_2O, 200 mmol) tetrafluoroboric acid yielded the crude product as fine white needles. After washing, it was recrystallized from diethyl ether.

Intercalation/Chemical Exfoliation. Under argon atmosphere, 1.5 mL *n*-BuLi (2.0 M) in cyclohexane was added to 1.5 g (9.4 mmol) MoS_2. After the addition of 10 mL of dry hexane as solvent, the dispersion was heated to 65 °C overnight. Then, 100 mL of distilled water was added to the cooled reaction mixture under hydrogen evolution. After the decrease of the gas formation, organic impurities were removed by extraction with hexane (two times), and the aqueous phase was collected. A portion of the concentrated black aqueous phase was diluted further with distilled water to obtain a yellowish-brown dispersion which was bath-sonicated for 20 min at 50 °C and precentrifuged at 750 rpm (62 *g*) for 1.5 h at 20 °C in order to remove nonexfoliated material as sediment. Four further centrifugation steps at 14 krpm (21 475 g, 1.5 h, 20 °C) removed very small MoS_2 material and LiOH generated during the reaction as supernatant. After each high speed centrifugation step, the sediment was collected with fresh distilled water, shaken by hand and subjected to the next centrifugation step. After the washing procedure, the final sediment was redispersed in distilled water by bath sonication (30 min, 50 °C) yielding a highly stable dispersion. To obtain *CE*-MoS_2 predominantly as 1T polytype, 1.5 g of MoS_2 and 15 mL of *n*-BuLi (2.0 M) were used for intercalation. The material thus obtained is denoted as 1T *CE*-MoS_2. Unless otherwise noted, *CE*-MoS_2 refers to the chemically exfoliated material obtained from intercalation using excess MoS_2.

Functionalization. 4-Methoxyphenyldiazonium tetrafluoroborate dissolved in distilled water was added to the dilute yellowish/brownish purified *CE*-MoS_2 dispersion dropwise under exposure to light. After addition of only a few drops of reagent, a black precipitate formed. The reaction mixture was stirred overnight and filtered through a 0.2 μm reinforced cellulose membrane filter (Sartorius). Washing with isopropyl

alcohol to remove organic side products and with distilled water yielded the functionalized MoS_2 product after drying under vacuum.

Characterization. Optical extinction was measured on a PerkinElmer Lambda 1050 in quartz cuvettes with a path length of 0.4 cm. Raman spectroscopy was performed using a Horiba Scientific LabRAM Aramis equipped with a motorized sample holder. TGA-MS analysis was carried out on a Netzsch STA 409 CD with EI ion source and quadrupole mass spectrometer on a 10 K/min temperature ramp using helium as inert gas. Zeta potential measurements were carried out on a Malvern Zetasizer Nano system with irradiation from a 633 nm He−Ne laser. X-ray photoelectron spectroscopy was performed under ultrahigh vacuum conditions ($<5 \times 10^{-10}$ mbar), using monochromated Al Kα X-rays (1486.6 eV) from an Omicron XM1000 MkII X-ray source and an Omicron EA125 energy analyzer. An Omicron CN10 electron flood gun was used for charge compensation and the binding energy scale was referenced to the adventitious carbon 1s core-level at 284.8 eV. Mo 3d and S 2p core-level regions were recorded at an analyzer pass energy of 15 eV and with slit widths of 6 mm (entry) and 3 mm × 10 mm (exit), resulting in an instrumental resolution of 0.48 eV. After subtraction of a Shirley background, the core-level spectra were fitted with Gaussian−Lorentzian line shapes and using Marquardt's algorithm. IR spectra were acquired using a PerkinElmer Frontier spectrometer equipped with a diffuse reflectance unit and CsI as matrix. Atomic force microscopy (AFM) was carried out on a Solver Pro scanning probe microscope (NT-MDT) equipped with a Sony Exwave HAD camera optical zoom (6.5) in tapping mode. Low resolution bright field transmission electron microscopy (TEM) imaging was performed using a JEOL 2100, operated at 200 kV on holey carbon grids (400 mesh). Prior to HRTEM imaging, the samples were drop-cast onto grids that were then kept at 120 °C overnight under vacuum to remove excess surfactant. HRTEM imaging was then performed on an FEI Titan TEM operated at 300 kV. The network transistor devices based on region-selective assembly of *CE*-MoS_2 were prepared in analogy to reference[53] (see also Supporting Information). In brief, the prepatterned chip is immersed in 0.2 mM isopropyl alcohol solution of 12-mercaptododecylphosphonic acid (HS-C_{12}−PA) for 70 h to form the nonpolar self-assembled monolayer (SAM). The SAM in the channel region is removed with O_2 plasma and replaced by the positively charged SAM 3-methyl-1-(12-phosphonododecyl) imidazolium bromide. *CE*-MoS_2 in aqueous solution is selectively deposited by dip-coating for 24 h.

Modeling. The simulation scheme adopted throughout this work is based on Density Functional Theory (DFT) as implemented in AIMS and CP2K codes.[57] PBE[58] exchange and correlation functional with van der Waals correction at the Grimme-D3 level[59] has been used. In CP2K, the wave functions are expanded on a Gaussian basis set, whereas an auxiliary plane-wave expansion of the electronic density is used to efficiently evaluate the Hartree part of the Coulomb interactions and the exchange-correlation energy. Goedecker-type pseudopotentials are used for all atoms with triple-ζ plus polarization (TZVP) Gaussian basis sets. A kinetic cutoff of 300 Ryd is used for the plane-wave expansion of the electronic density and BZ integration is restricted to the Γ-point. The geometry is relaxed until the maximum force on each atom is less than 0.01 eV/Ang.

To model both the clean and functionalized MoS_2 monolayers, we used hexagonal cells obtained replicating 6 × 6 times the hexagonal MoS_2 unit cell, with 1T symmetry and lattice parameter $a = 3.16$ Å. The use of this cell guarantees a sampling of the Brillouin zone which leads to an error on the evaluation of total energy smaller than 0.001 eV/cell. Different images of the monolayer along z are separated by a vacuum region of approximately 45 Å. Neutral and charged (with $-1\,|e|$ and $-4\,|e|$ excess charge) substrates have been compared. An energy correction for multipole error in Hartree potential has been added.

Conflict of Interest: The authors declare no competing financial interest.

Supporting Information Available: Purification of *CE*-MoS_2, comparison of intercalation conditions, further characterization of functionalized MoS_2 (zeta potential, Raman, XPS, XRD), details on redispersion experiments, functionalization of chemically exfoliated MoS_2 from intercalation using excess *n*-BuLi, functionalization after deposition on substrates, details DFT calculations. The Supporting Information is available free of charge on the ACS Publications website at DOI: 10.1021/acsnano.5b00965.

Acknowledgment. The research leading to these results has received funding from the European Union Seventh Framework Program under Grant Agreement No. 604391 Graphene Flagship. In addition, C.B. acknowledges the German research foundation DFG (BA 4856/1-1). J.N.C. acknowledges the European Research Council Grant SEMANTICS and SFI (11/PI/1087) for financial support. K.C.K., I.A., P.V., F.H., A.H., Z.W. and M.H. acknowledge the Collaborative Research Centre SFB953 "Synthetic Carbon Allotropes". K.C.K. acknowledges the Erlangen Graduate School Molecular Science (GSMS). H.C.N. and V.N. acknowledge ERC 2DNanoCaps, SFI PIYRA and FP7 MoWSeS. G.S.D., N.McE., and N.C.B. acknowledge SFI for PI_10/IN.1/I3030. Z.W. and M.H. acknowledge the Cluster of Excellence "Engineering of Advanced Materials". S.S. and C.S.C. have been supported by the European Research Council (Quest project). All calculations were performed on the Parsons cluster maintained by the Trinity Centre for High Performance Computing, under project ID: HPC_12_0722. This cluster was funded through grants from Science Foundation Ireland.

REFERENCES AND NOTES

1. Wang, Q. H.; Kalantar-Zadeh, K.; Kis, A.; Coleman, J. N.; Strano, M. S. Electronics and Optoelectronics of Two-Dimensional Transition Metal Dichalcogenides. *Nat. Nanotechnol.* **2012**, *7*, 699–712.
2. Butler, S. Z.; Hollen, S. M.; Cao, L.; Cui, Y.; Gupta, J. A.; Gutierrez, H. R.; Heinz, T. F.; Hong, S. S.; Huang, J.; Ismach, A. F.; et al. Progress, Challenges, and Opportunities in Two-Dimensional Materials Beyond Graphene. *ACS Nano* **2013**, *7*, 2898–2926.
3. Chhowalla, M.; Shin, H. S.; Eda, G.; Li, L.-J.; Loh, K. P.; Zhang, H. The Chemistry of Two-Dimensional Layered Transition Metal Dichalcogenide Nanosheets. *Nat. Chem.* **2013**, *5*, 263–275.
4. Nicolosi, V.; Chhowalla, M.; Kanatzidis, M. G.; Strano, M. S.; Coleman, J. N. Liquid Exfoliation of Layered Materials. *Science* **2013**, *340*, 1420.
5. Xu, M.; Liang, T.; Shi, M.; Chen, H. Graphene-like Two-Dimensional Materials. *Chem. Rev.* **2013**, *113*, 3766–3798.
6. Novoselov, K. S.; Fal'ko, V. I.; Colombo, L.; Gellert, P. R.; Schwab, M. G.; Kim, K. A Roadmap for Graphene. *Nature* **2012**, *490*, 192–200.
7. Osada, M.; Sasaki, T. Exfoliated Oxide Nanosheets: New Solution to Nanoelectronics. *J. Mater. Chem.* **2009**, *19*, 2503–2511.
8. Reich, E. S. Phosphorene Excites Materials Scientists. *Nature* **2014**, *506*, 19–19.
9. Zhan, Y. J.; Liu, Z.; Najmaei, S.; Ajayan, P. M.; Lou, J. Large-Area Vapor-Phase Growth and Characterization of MoS_2 Atomic Layers on a SiO_2 Substrate. *Small* **2012**, *8*, 966–971.
10. Berkdemir, A.; Gutierrez, H. R.; Botello-Mendez, A. R.; Perea-Lopez, N.; Elias, A. L.; Chia, C.-I.; Wang, B.; Crespi, V. H.; Lopez-Urias, F.; Charlier, J.-C.; et al. , Identification of Individual and Few Layers of WS_2 Using Raman Spectroscopy. *Sci. Rep.* **2013**, *3*, 1755.
11. Eda, G.; Yamaguchi, H.; Voiry, D.; Fujita, T.; Chen, M.; Chhowalla, M. Photoluminescence from Chemically Exfoliated MoS_2. *Nano Lett.* **2011**, *11*, 5111–5116.
12. Coleman, J. N.; Lotya, M.; O'Neill, A.; Bergin, S. D.; King, P. J.; Khan, U.; Young, K.; Gaucher, A.; De, S.; Smith, R. J.; et al. Two-Dimensional Nanosheets Produced by Liquid Exfoliation of Layered Materials. *Science* **2011**, *331*, 568–571.
13. Smith, R. J.; King, P. J.; Lotya, M.; Wirtz, C.; Khan, U.; De, S.; O'Neill, A.; Duesberg, G. S.; Grunlan, J. C.; Moriarty, G.; et al. Large-Scale Exfoliation of Inorganic Layered Compounds in Aqueous Surfactant Solutions. *Adv. Mater.* **2011**, *23*, 3944–3948.
14. Backes, C.; Smith, R. J.; McEvoy, N.; Berner, N. C.; McCloskey, D.; Nerl, H. C.; O'Neill, A.; King, P. J.; Higgins, T.; Hanlon, D.; et al.

Edge and Confinement Effects Allow *in situ* Measurement of Size and Thickness of Liquid-Exfoliated Nanosheets. *Nature Commun.* **2014**, *5*, 4576.
15. Kuila, T.; Bose, S.; Mishra, A. K.; Khanra, P.; Kim, N. H.; Lee, J. H. Chemical Functionalization of Graphene and Its Applications. *Prog. Mater. Sci.* **2012**, *57*, 1061–1105.
16. Sun, Z.; James, D. K.; Tour, J. M. Graphene Chemistry: Synthesis and Manipulation. *J. Phys. Chem. Lett.* **2011**, *2*, 2425–2432.
17. Englert, J. M.; Dotzer, C.; Yang, G.; Schmid, M.; Papp, C.; Gottfried, J. M.; Steinrueck, H.-P.; Spiecker, E.; Hauke, F.; Hirsch, A. Covalent Bulk Functionalization of Graphene. *Nat. Chem.* **2011**, *3*, 279–286.
18. Cui, Z. H.; Oyer, A. J.; Glover, A. J.; Schniepp, H. C.; Adamson, D. H. Large Scale Thermal Exfoliation and Functionalization of Boron Nitride. *Small* **2014**, *10*, 2352–2355.
19. Sainsbury, T.; Satti, A.; May, P.; O'Neill, A.; Nicolosi, V.; Gun'ko, Y. K.; Coleman, J. N. Covalently Functionalized Hexagonal Boron Nitride Nanosheets by Nitrene Addition. *Chem.—Eur. J.* **2012**, *18*, 10808–10812.
20. Sainsbury, T.; Satti, A.; May, P.; Wang, Z.; McGovern, I.; Gun'ko, Y. K.; Coleman, J. Oxygen Radical Functionalization of Boron Nitride Nanosheets. *J. Am. Chem. Soc.* **2012**, *134*, 18758–18771.
21. Makarova, M.; Okawa, Y.; Aono, M. Selective Adsorption of Thiol Molecules at Sulfur Vacancies on MoS_2(0001), Followed by Vacancy Repair *via* S−C Dissociation. *J. Phys. Chem. C* **2012**, *116*, 22411–22416.
22. Chou, S. S.; De, M.; Kim, J.; Byun, S.; Dykstra, C.; Yu, J.; Huang, J.; Dravid, V. P. Ligand Conjugation of Chemically Exfoliated MoS_2. *J. Am. Chem. Soc.* **2013**, *135*, 4584–4587.
23. Zhou, L.; He, B.; Yang, Y.; He, Y. Facile Approach to Surface Functionalized MoS_2 Nanosheets. *RSC Adv.* **2014**, *4*, 32570–32578.
24. Georgakilas, V.; Otyepka, M.; Bourlinos, A. B.; Chandra, V.; Kim, N.; Kemp, K. C.; Hobza, P.; Zboril, R.; Kim, K. S. Functionalization of Graphene: Covalent and Non-Covalent Approaches, Derivatives and Applications. *Chem. Rev.* **2012**, *112*, 6156–6214.
25. Voiry, D.; Goswami, A.; Kappera, R.; SilvaCecilia de Carvalho Castro, e.; Kaplan, D.; Fujita, T.; Chen, M.; Asefa, T.; Chhowalla, M. Covalent Functionalization of Monolayered Transition Metal Dichalcogenides by Phase Engineering. *Nat. Chem.* **2014**, *7*, 45–49.
26. Benavente, E.; Santa Ana, M. A.; Mendizábal, F.; González, G. Intercalation Chemistry of Molybdenum Disulfide. *Coord. Chem. Rev.* **2002**, *224*, 87–109.
27. Marseglia, E. A. Transition Metal Dichalcogenides and Their Intercalates. *Int. Rev. Phys. Chem.* **1983**, *3*, 177–216.
28. Wypych, F.; Schollhorn, R. 1T-MoS_2, a New Metallic Modification of Molybdenum Disulfide. *J. Chem. Soc., Chem. Commun.* **1992**, 1386–1388.
29. Marseglia, E. A. Transition Metal Dichalcogenides and Their Intercalates. *Int. Rev. Phys. Chem.* **1983**, *3*, 177–216.
30. Joensen, P.; Frindt, R. F.; Morrison, S. R. Single-Layer MoS_2. *Mater. Res. Bull.* **1986**, *21*, 457–461.
31. Gatensby, R.; McEvoy, N.; Lee, K.; Hallam, T.; Berner, N. C.; Rezvani, E.; Winters, S.; O'Brien, M.; Duesberg, G. S. Controlled Synthesis of Transition Metal Dichalcogenide Thin Films for Electronic Applications. *Appl. Surf. Sci.* **2014**, *297*, 139–146.
32. Wilson, J. A.; Yoffe, A. D. Transition Metal Dichalcogenides. Discussion and Interpretation of the Observed Optical, Electrical, and Structural Properties. *Adv. Phys.* **1969**, *18*, 193–335.
33. Chou, S. S.; Kaehr, B.; Kim, J.; Foley, B. M.; De, M.; Hopkins, P. E.; Huang, J.; Brinker, C. J.; Dravid, V. P. Chemically Exfoliated MoS_2 as near-Infrared Photothermal Agents. *Angew. Chem., Int. Ed.* **2013**, *52*, 4160–4164.
34. Schumacher, A.; Scandella, L.; Kruse, N.; Prins, R. Single-Layer MoS_2 on Mica: Studies by Means of Scanning Force Microscopy. *Surf. Sci. Lett.* **1993**, *289*, L595–L598.
35. Zeng, Z.; Yin, Z.; Huang, X.; Li, H.; He, Q.; Lu, G.; Boey, F.; Zhang, H. Single-Layer Semiconducting Nanosheets: High-Yield Preparation and Device Fabrication. *Angew. Chem., Int. Ed.* **2011**, *50*, 11093–11097.
36. Strano, M. S.; Dyke, C. A.; Usrey, M. L.; Barone, P. W.; Allen, M. J.; Shan, H.; Kittrell, C.; Hauge, R. H.; Tour, J. M.; Smalley, R. E. Electronic Structure Control of Single-Walled Carbon Nanotube Functionalization. *Science* **2003**, *301*, 1519–1522.
37. Lomeda, J. R.; Doyle, C. D.; Kosynkin, D. V.; Hwang, W.-F.; Tour, J. M. Diazonium Functionalization of Surfactant-Wrapped Chemically Converted Graphene Sheets. *J. Am. Chem. Soc.* **2008**, *130*, 16201–16206.
38. Pagona, G.; Karousis, N.; Tagmatarchis, N. Aryl Diazonium Functionalization of Carbon Nanohorns. *Carbon* **2008**, *46*, 604–610.
39. Ulbricht, H.; Zacharia, R.; Cindir, N.; Hertel, T. Thermal Desorption of Gases and Solvents from Graphite and Carbon Nanotube Surfaces. *Carbon* **2006**, *44*, 2931–2942.
40. Golub, A. S.; Shumilova, I. B.; Novikov, Y. N.; Mansot, J. L.; Danot, M. Phenanthroline Intercalation into Molybdenum Disulfide. *Solid State Ionics* **1996**, *91*, 307–314.
41. Li, H.; Zhang, Q.; Yap, C. C. R.; Tay, B. K.; Edwin, T. H. T.; Olivier, A.; Baillargeat, D. From Bulk to Monolayer MoS_2: Evolution of Raman Scattering. *Adv. Funct. Mater.* **2012**, *22*, 1385–1390.
42. Terrones, H.; Corro, E. D.; Feng, S.; Poumirol, J. M.; Rhodes, D.; Smirnov, D.; Pradhan, N. R.; Lin, Z.; Nguyen, M. A. T.; Elias, A. L.; et al. , New First Order Raman-Active Modes in Few Layered Transition Metal Dichalcogenides. *Sci. Rep.* **2014**, *4*, 4215.
43. Chen, J. M.; Wang, C. S. Second Order Raman Spectrum of MoS_2. *Solid State Commun.* **1974**, *14*, 857–860.
44. Sekine, T.; Uchinokura, K.; Nakashizu, T.; Matsuura, E.; Yoshizaki, R. Dispersive Raman Mode of Layered Compound 2H-MoS_2 under the Resonant Condition. *J. Phys. Soc. Jpn.* **1984**, *53*, 811–818.
45. Stacy, A. M.; Hodul, D. T. Raman Spectra of IVb and VIb Transition Metal Disulfides Using Laser Energies near the Absorption Edges. *J. Phys. Chem. Solids* **1985**, *46*, 405–409.
46. Jimenez Sandoval, S.; Yang, D.; Frindt, R. F.; Irwin, J. C. Raman Study and Lattice Dynamics of Single Molecular Layers of Molybdenum Disulfide. *Phys. Rev. B: Condens. Matter* **1991**, *44*, 3955–62.
47. Hesse, M.; Meier, H.; Zeeh, B. *Spectroscopic Methods in Organic Chemistry*; Thieme Medical Publishers: Stuttgart, 2008.
48. Cunningham, G.; Lotya, M.; Cucinotta, C. S.; Sanvito, S.; Bergin, S. D.; Menzel, R.; Shaffer, M. S. P.; Coleman, J. N. Solvent Exfoliation of Transition Metal Dichalcogenides: Dispersibility of Exfoliated Nanosheets Varies Only Weakly between Compounds. *ACS Nano* **2012**, *6*, 3468–3480.
49. O'Neill, A.; Khan, U.; Coleman, J. N. Preparation of High Concentration Dispersions of Exfoliated MoS_2 with Increased Flake Size. *Chem. Mater.* **2012**, *24*, 2414–2421.
50. Wang, Y.; Ou, J. Z.; Balendhran, S.; Chrimes, A. F.; Mortazavi, M.; Yao, D. D.; Field, M. R.; Latham, K.; Bansal, V.; Friend, J. R.; et al. Electrochemical Control of Photoluminescence in Two-Dimensional MoS_2 Nanoflakes. *ACS Nano* **2013**, *7*, 10083–10093.
51. Shmeliov, A.; Shannon, M.; Wang, P.; Kim, J. S.; Okunishi, E.; Nellist, P. D.; Dolui, K.; Sanvito, S.; Nicolosi, V. Unusual Stacking Variations in Liquid-Phase Exfoliated Transition Metal Dichalcogenides. *ACS Nano* **2014**, *8*, 3690–3699.
52. Wang, Z.; Mohammadzadeh, S.; Schmaltz, T.; Kirschner, J.; Khassanov, A.; Eigler, S.; Mundloch, U.; Backes, C.; Steinrück, H.-G.; Magerl, A.; et al. Region-Selective Self-Assembly of Functionalized Carbon Allotropes from Solution. *ACS Nano* **2013**, *7*, 11427–11434.
53. Wang, Z.; Eigler, S.; Halik, M. Scalable Self-Assembled Reduced Graphene Oxide Transistors on Flexible Substrate. *Appl. Phys. Lett.* **2014**, *104*, 24350.
54. Kirschner, J.; Wang, Z.; Eigler, S.; Steinruck, H.-P.; Jager, C. M.; Clark, T.; Hirsch, A.; Halik, M. Driving Forces for the Self-Assembly of Graphene Oxide on Organic Monolayers. *Nanoscale* **2014**, *6*, 11344–11350.
55. Moses, P. G.; Mortensen, J. J.; Lundqvist, B. I.; Nørskov, J. K. Density Functional Study of the Adsorption and van der Waals Binding of Aromatic and Conjugated Compounds

on the Basal Plane of MoS_2. *J. Chem. Phys.* **2009**, *130*, 104709.
56. Henkelman, G.; Arnaldsson, A.; Jónsson, H. A Fast and Robust Algorithm for Bader Decomposition of Charge Density. *Comput. Mater. Sci.* **2006**, *36*, 354–360.
57. VandeVondele, J.; Krack, M.; Mohamed, F.; Parrinello, M.; Chassaing, T.; Hutter, J. Quickstep: Fast and Accurate Density Functional Calculations Using a Mixed Gaussian and Plane Waves Approach. *Comput. Phys. Commun.* **2005**, *167*, 103–128.
58. Perdew, J. P.; Burke, K.; Ernzerhof, M. Generalized Gradient Approximation Made Simple. *Phys. Rev. Lett.* **1996**, *77*, 3865–3868.
59. Grimme, S.; Antony, J.; Ehrlich, S.; Krieg, H. A Consistent and Accurate *ab initio* Parametrization of Density Functional Dispersion Correction (DFT-D) for the 94 Elements H-Pu. *J. Chem. Phys.* **2010**, *132*, 154104.